References and notes

1. Fujishima, A.; Honda, K. *Nature* **1972**, *238*, 37.
2. Fujishima, A.; Rao, T. N.; Try, D. A. *J. Photochem. Photobiol. C* **2000**, *1*, 1.
3. Christensen, P. A.; Curtis, T. P.; Egerton, T. A.; Kosa, S. A. M.; Tinlin, J. R. *Appl. Catal., B* **2003**, *41*, 371.
4. Bekbolet, M. *Water Sci. Technol.* **1997**, *35*, 95.
5. Cai, R.; Kubota, Y.; Shuin, T.; Sakai, H.; Hashimoto, K.; Fujishima, A. *Cancer Res.* **1992**, *52*, 2346.
6. Kubota, Y.; Shuin, T.; Kawasaki, C.; Hosaka, M.; Kitamura, H.; Cai, R.; Sakai, H.; Hashimoto, K.; Fujishima, A. *Br. J. Cancer* **1994**, *70*, 1107.
7. Fujishima, A.; Zhang, X. *C.R. Chim.* **2006**, *9*, 750.
8. Shimizu, N.; Ogino, C.; Dadjour, M. F.; Murata, T. *Ultrason. Sonochem.* **2007**, *14*, 184.
9. Harada, H. *Ultrason. Sonochem.* **2001**, *8*, 55.
10. Berberidou, C.; Poulios, I.; Xekoukoulotakis, N. P.; Mantzavinos, D. *Appl. Catal., B* **2007**, *74*, 63.
11. Dadjour, M. F.; Ogino, C.; Matsumura, S.; Shimizu, N. *Biochem. Eng. J.* **2005**, *25*, 243.
12. Dadjour, M. F.; Ogino, C.; Matsumura, S.; Nakamura, S.; Shimizu, N. *Water Res.* **2006**, *40*, 1137.
13. Ogino, C.; Dadjour, M. F.; Takaki, K.; Shimizu, N. *Biochem. Eng. J.* **2006**, *32*, 100.
14. Szeimies, R. M.; Landthaler, M. *Recent Results Cancer Res.* **2002**, *160*, 240.
15. Silva, J. N.; Filipe, P.; Morliere, P.; Maziere, J. C.; Freitas, J. P.; Cirne, d. e.; Castro, J. L.; Santus, R. *Biomed. Mater. Eng.* **2006**, *16*, 147.
16. Roots, R.; Okada, S. *Radiat. Res.* **1975**, *64*, 306.
17. Chadwick, M. D.; Goodwin, J. W.; Lawson, E. J.; Mills, P. D. A.; Vincent, B. *Colloids Surf., A* **2002**, *203*, 229.
18. Kanehira, K.; Banzai, T.; Ogino, C.; Shimizu, N.; Kubota, Y.; Sonezaki, S. *J. Colloid Interface Sci.* **2008**, *64*, 10.
19. Pettersson, A.; Marino, G.; Pursiheimo, A.; Rosenholm, J. B. *J. Colloid Interface Sci.* **2000**, *228*, 73.
20. Yamada, T.; Iwasaki, Y.; Tada, H.; Iwabuki, H.; Chuah, M. K.; VandenDriessche, T.; Fukuda, H.; Kondo, A.; Ueda, M.; Seno, M.; Tanizawa, K.; Kuroda, S. *Nat. Biotechnol.* **2003**, *21*, 885.
21. Kasuya, T.; Yamada, T.; Ueda, A.; Matsuzaki, T.; Okajima, T.; Tatematsu, K.; Tanizawa, K.; Kuroda, S. *J. Biosci. Bioeng.* **2008**, *106*, 99.
22. Flory, P.J. Cornel University Press: Ithaca, NY, 1953.

ELSEVIER

Affibody-displaying bionanocapsules for specific drug delivery to HER2-expressing cancer cells

Takuya Shishido [a], Hiroaki Mieda [a], Sang Youn Hwang [b], Yuya Nishimura [a], Tsutomu Tanaka [b], Chiaki Ogino [a], Hideki Fukuda [b], Akihiko Kondo [a,*]

[a] Department of Chemical Science and Engineering, Graduate School of Engineering, Kobe University, 1-1 Rokkodaicho, Nada-ku, Kobe 657-8501, Japan
[b] Organization of Advanced Science and Technology, Kobe University, 1-1 Rokkodaicho, Nada-ku, Kobe 657-8501, Japan

ABSTRACT

A novel HER2-targeted carrier was developed using bionanocapsules (BNCs). Bionanocapsules (BNCs) are 100-nm hollow nanoparticles composed of the L-protein of hepatitis B virus surface antigen. An affibody of HER2 was genetically displayed on the BNC surface (Z_{HER2}–BNC). For the investigation of binding affinity, Z_{HER2}–BNC was incubated with the cancer cell lines SK-BR-3 (HER2 positive), and MDA-MB-231 (HER2 negative). For analysis of HER2 targeting specificity, Z_{HER2}–BNC or Z_{WT}–BNC (without affibody) was incubated with both SK-BR-3 and MDA-MB-231 cells by time lapse and concentration. For the delivery of encapsulated molecules (calcein), fluorescence of Z_{HER2}–BNC mixed with liposomes was also compared with that of Z_{WT}–BNC and nude liposomes by incubation with SK-BR-3 cells. As a result, Z_{HER2}–BNC-liposome complex demonstrated the delivery to HER2-expressing cells (SK-BR-3) with a high degree of specificity. This indicates that genetically engineered BNCs are promising carrier for cancer treatment.

© 2010 Elsevier Ltd. All rights reserved.

Most of studies about drug delivery system (DDS) are focused on three points; enhancement of targeting efficiency,[1] increase of drug encapsulation yield,[2] and effective release of drug into the target cell.[3] Among these topics, the research on improving target-efficiency is the most active field such as materials for carrier and homing molecule immobilization technique for active targeting. Although viral system is known as effective to target and deliver, there are limitations about safety problem such as high immunogenicity and possibility of introducing foreign viral gene. Therefore, the development of novel carrier should be required.

A bionanocapsule (BNC) is composed of hepatitis B virus (HBV) surface antigen (HBsAg) L-protein combined with a lipid bilayer derived from yeast endoplasmic reticulum (ER) membrane.[4] Bionanocapsules are attractive as carriers for targeted drug delivery due to their high stability in the blood, high internalized efficiency compared with original HBV, high capacity, and high specificity for human hepatocytes.[5–7] However, a BNC has original specificity only for hepatocytes. To surmount this limited targeting, the pre-S region (a human hepatocyte recognizing molecule) is genetically substituted with other bio-recognizable molecules, such as epidermal growth factor (EGF) or cell penetrating peptide (CPP).[5,8] However, the range of complex ligands that can be displayed on the

surface of a BNC is limited. There is considerable interest in development of novel targeting molecules that are both simple in structure and have high specificity that can be engineered onto BNCs.

We focused on using affibodies as targeting molecules for BNC-mediated drug delivery. Affibodies are a new class of affinity ligands derived from one of the IgG-binding domains of staphylococcal protein A. Affibody molecules have simple and robust structures with lower molecular weight (6 kDa) than antibodies (about 150 kDa), and have both high binding affinity and high specificity. Affibody molecules that can bind a range of different proteins, such as insulin, TNF-α, EGFR, and HER2, have been identified.[9] HER2 (ErbB2) is a member of the human epidermal growth factor receptor (EGFR) family, and is highly expressed in several types of cancer, especially tumors of the breast (30%), and ovary (15–30%).[10,11] Over-expression of HER2 is associated with resistance to chemotherapy and poor prognosis,[12,13] thus making HER2 an attractive target for molecular therapy.[14–16] Among HER2-binding affibody variants, $Z_{HER2:342}$ shows very high affinity ($K_D \sim 22$ pM), and it has been applied to various carriers, including liposomes,[17] nanoparticles,[18] biopolymers,[19] and the adenovirus vector.[20] In this study, we constructed $Z_{HER2:342}$ displaying BNCs (Z_{HER2}–BNC) by genetically substituted the pre-S region with Z_{HER2} and the affibody-displaying BNCs-assisted drug delivery was demonstrated.

The plasmid construction and BNC preparation were carried out as follows. The pGLDLIIP39-RcT plasmid contains the HBV

envelope L gene.[4] A fragment encoding GLD promoter and cloning sites was amplified using pGLDLIIP39-RcT as a template. The primers utilized were 5′-GGGAGATCTGCGAGCTTACCAGTTCTCAC-3′ and 5′-GGGGCGGCCGCGGATCCCCGCGGTGTTTTTATACTCGACCTCG-3′. The amplified fragment was digested with BglII/NotI and ligated into BamHI/NotI sites in pGLDLd50.[8] The resulting plasmid was named pGLDsLd (1–159). The fragment encoding the chicken-lysozyme signal peptide and a part of L gene (from 1 to 49 a.a.) was subsequently amplified from pGLDLIIP39-RcT using the following primers: 5′-GGGCCGCGGATGAGATCTTTGTTGATCTT-3′ and 5′-GG GGCGGCCGCCGGATCCACCCGCTCCTACCTGATTTGCCT-3′. The amplified fragment was digested with SacII/NotI and ligated into pGLDsLd (1–159). The resulting plasmid was named pGLDsLd50. The gene encoding synthetic EZ, which consists of the first six amino acids of domain E and Z derived from Staphylococcus aureus protein A, was amplified from pXIHAbla-Ld33-ZZ-EGFP[21] using the following primers: 5′-GGGGGATCCGCGCAACACGACGAAGC CGTAGACAACAAATTCAACAA-3′ and 5′-GGGGCGGCCGCCTTTCGGC GCCTGAGCATCAT-3′. The amplified fragment was digested with

BamHI/NotI and ligated into pGLDsLd50. The resultant plasmid was named pGLDsLd50-Z$_{WT}$. The gene encoding amino acid residues 1–25 of EZ$_{HER2:342}$, which includes the E domain and the two α-helix of the Z$_{HER2:342}$ domain, was prepared by annealing the following synthetic oligonucleotides: 5′-GTAGACAACAAATT CAACAAAGAAATGAGAAACGCGTACTGGGAGATCGCTTTGTTACCTAA CTTAAACAACCAA-3′ and 5′-TTGGTTGTTTAAGTTAGGTAACAAAGC GATCTCCCAGTACGCGTTTCTCATTTCTTTGTTGAATTTGTTGTCTAC-3′. A fragment encoding residues 19–58 of EZ$_{HER2:342}$, which includes the third α-helix of the Z$_{HER2:342}$ domain, was amplified from pGLDsLd50-Z$_{WT}$ using the following primers: 5′-TTACCTAACTT AAACAACCAACAAAAGAGAGCCTTCATCAGAAGTTTATACGATGACCC AAGCCAAAGCGC-3′ and 5′-GGGGCGGCCGCCTTTCGGCGCCTGAG CATCAT-3′. Both amplified fragments were mixed and PCR was carried out using the following primers: 5′-GGGGGATCCGCGCAA CACGACGAAGCCGTAGACAACAAATTCAACAA-3′ and 5′-GGGGCGGC CGCCTTTCGGCGCCTGAGCATCAT-3′. The amplified fragment encoding EZ$_{HER2:342}$ in its entirety was digested with BamHI/NotI and ligated into pGLDsLd50. The resulting plasmid was designated
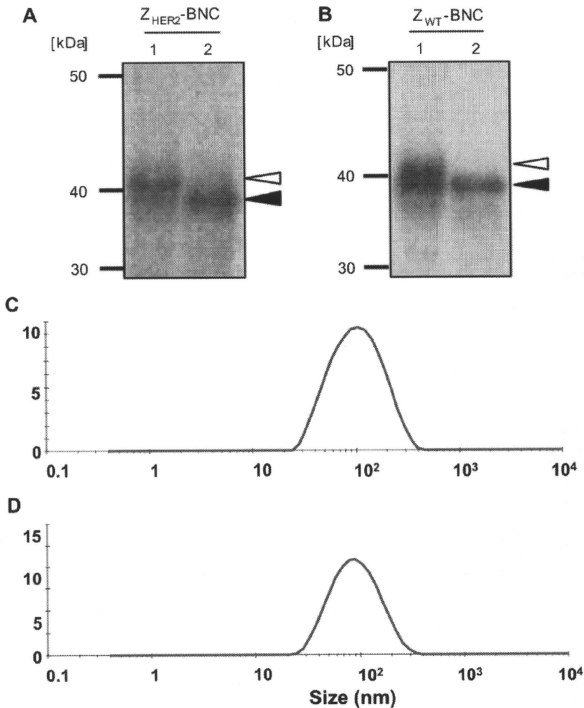

Figure 1. Western blot analysis and DLS of affibody-displaying BNCs. Purified affibody-displaying BNCs were analyzed with anti-HBsAg antibody. (A) Lane 1: Z$_{HER2}$-BNCs; Lane 2: PNGase F-treated Z$_{HER2}$-BNCs. (B) Lane 1: Z$_{WT}$-BNCs; Lane 2: PNGase F-treated Z$_{WT}$-BNCs. The two bands detected corresponded to unglycosylated (closed arrow) and glycosylated (opened arrow) forms of each affibody-displaying BNC. (C) Size distribution of Z$_{HER2}$-BNC. (D) Size distribution of Z$_{WT}$-BNC
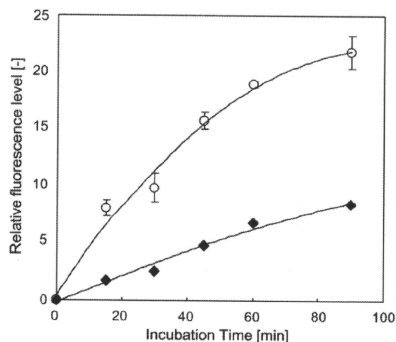
Figure 2. Time course of cellular uptake of Z_{HER2}-BNC into SK-BR-3 and MDA-MB-231 cells. Cells were incubated with Alexa488-labeled Z_{HER2}-BNC (final concentration: 1.0 μM) for 15, 30, 60, and 90 min. After washing three times with serum-free medium, cells was recovered and assayed by flow cytometry. Fluorescence intensity is given as the mean and standard deviation of three independent experiments. Open circle: SK-BR-3, Closed square: MDA-MB-231.

pGLDsLd50-Z_{HER2}. Z_{HER2}-BNCs and Z_{WT}-BNCs were obtained according to the previously described methods.[4]

Purified Z_{HER2}-BNCs were analyzed by western blot using anti-HbsAg (Fig. 1A and B). Two major bands were detected in each western blot analysis, which might have been caused by glycosylation of HbsAg.[4] The yield from 1 L of yeast culture was 2.80 mg of Z_{HER2}-BNCs and 3.50 mg of Z_{WT}-BNCs, a more efficient recovery that than reported for other genetically engineered BNCs.[5,8] The diameter of the affibody-displaying BNCs analyzed by dynamic light scattering was about 100 nm (Fig. 1D),[22] suggesting that affibody-displaying BNCs formed nano-size particles and size distributions of both BNCs were almost same. This size is suitable for use as a circulating carrier, since particles larger than 150 nm in diameter are known to be easily removed by macrophages.

To evaluate cellular uptake of Z_{HER2}-BNCs, the HER2 over-expressing SK-BR-3 human breast cancer cells (approximately

10^6 HER2 molecules per cell) were incubated with Alexa488-labeled $Z_{HER2:342}$-BNCs. Purified Z_{HER2}-BNCs were reacted with Alexa Fluor 488 succinimidyl esters (Invitrogen) as previously described.[8] The Alexa488 number labeled to Z_{HER2}-BNCs or Z_{WT}-BNCs were over104 molecules/BNC (0.95 molecule/protein). SK-BR-3 cells were obtained from Riken BioResource Center (Tsukuba, Japan) and Human breast carcinoma MDA-MB-231 cells were obtained from Dainippon Sumitomo Pharma (Osaka, Japan) and served as negative control cells. The labeled Z_{HER2}-BNCs (final concentration: 1.0 μM) were added to each well and cultured. After washing with serum-free medium, the green fluorescence was analyzed by flow cytometry (Fig. 2). The green fluorescence signal was exited with a 488-nm blue laser and collected through a 530/30-nm band-pass filter. The fluorescence of Z_{HER2}-BNCs was detected after 15 min incubation, which is much faster than the appearance of WT-BNC fluorescence against to human liver carcinoma cell.[5–7] The binding rate of SK-BR-3 is three times higher than that of MDA-MB-231 cells. The fluorescence level increased along with the incubation time, and 60 min incubation was sufficient for binding of Z_{HER2}-BNCs to HER2 on the surface of SK-BR-3 cells, a result similar to that obtained with Z_{HER2}-molecules.[24] In contrast, the fluorescence of MDA-MB-231 cells increased only slightly after 60 min incubation.

The dose dependence of Z_{HER2}-BNCs for cellular uptake was similarly examined. SK-BR-3 cells were incubated with 0.1, 0.5, 1.0, and 2.5 μM Alexa488-labeled Z_{HER2}-BNCs or Z_{WT}-BNCs for 60 min (Fig. 3A). In the case of SK-BR-3 cells, fluorescence intensity increased obviously with the concentration of Z_{HER2}-BNCs. Fluorescence intensity of Z_{WT}-BNCs used as negative controls, increased slightly due to non-specific uptake. In the case of MDA-MB-231 cells, there was no difference in fluorescence of Z_{HER2}- and WT-BNCs, and it did not increase under the various conditions tested (Fig. 3B). These results clearly demonstrate that Z_{HER2}-BNCs specifically bind only to HER2 over-expressing cells.

Then internalization of Z_{HER2}-BNCs was examined using time-course analysis. SK-BR-3 and MDA-MB-231 cells were incubated for 30 min, 1 h, and 3 h with Z_{HER2}-BNCs (1.0 μM), washed with PBS, then observed by laser-scanning confocal microscopy (Fig. 4). Localization of Z_{HER2}-BNCs on the surface of SK-BR-3 cells was observed after 30 min incubation, a similar result to that observed using Z_{HER2}-molecules.[14,24] After 1 h incubation, Z_{HER2}-BNC internalization was observed, and internalization increased after 3 h incubation, a result consistent with that observed for anti-EGFR antibody-displaying BNCs.[21] Significant fluorescence in MDA-MB-
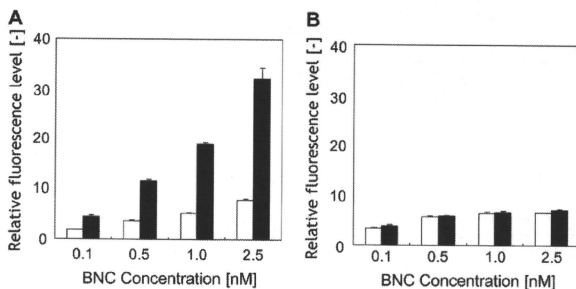
Figure 3. Dose dependence of Z_{HER2}-BNCs into (A) SK-BR-3 and (B) MDA-MB-231 cells. Cells were incubated with Alexa488-labeled Z_{HER2}-BNCs (final concentration: 0.1–2.5 μM) for 1 h. After washing three times with serum-free medium, cells were recovered and assayed by flow cytometry. The RLU (relative fluorescence level) is given as the mean and standard deviation of three independent experiments. Open bar: Z_{WT}-BNC; Closed bar: Z $_{HER2}$-BNC.
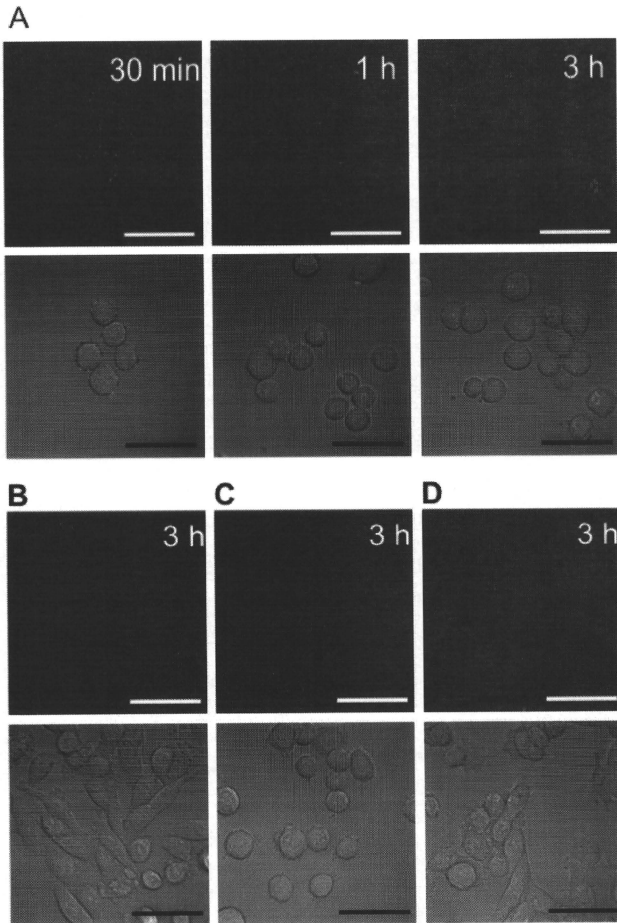
Figure 4. Fluorescence images of SK-BR-3 and MDA-MB-231 cells treated with affibody-displaying BNCs. Cells were incubated with 1.0 µM Alexa488-labeled Z_{HER2}-BNCs or Z_{WT}-BNCs. After incubation, cells were washed three times with serum-free medium and observed by laser-scanning confocal microscopy. (A) SK-BR-3 cells incubated with Z_{HER2}-BNCs for 30 min, 1 h, or 3 h. (B) MDA-MB-231 cells incubated with Z_{HER2}-BNCs for 3 h. (C) SK-BR-3 cells incubated with Z_{WT}-BNCs for 3 h. (D) MDA-MB-231 cells incubated with Z_{WT}-BNCs for 3 h. Scale bar = 50 µm.

231 cells was not observed even after 3 h incubation (Fig. 4B). In the case of Z_{WT}-BNCs, only slight fluorescence was observed from both SK-BR-3 and MDA-MB-231 cells (Fig. 4C and D). This result suggests that Z_{HER2}-BNCs have high specificity for HER2 and are capable of being efficiently internalized.

Encouraged by theses findings, we performed HER2-specific delivery using Z_{HER2}-BNCs. As a model compound, calcein was incorporated into Z_{HER2}-BNCs by the BNC–liposome complex method.[7] Briefly, freeze-dried liposomes (Coatsome EL-01-A, NOF, Tokyo, Japan) were dissolved in distilled water, and then the fluorescent material calcein (Dojindo, Kumamoto, Japan) was added (final concentration: 10 mM) and incubated for about 1 h at room temperature. Almost all liposomes might contain calcein inside because that excess amount of calcein was added during liposome
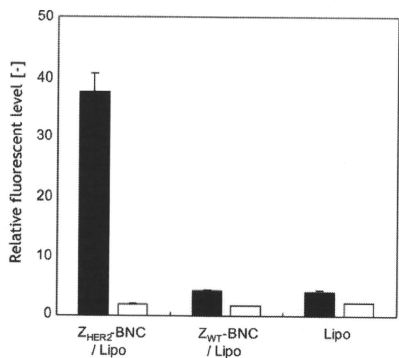
Figure 5. Transduction efficiency of calcein delivery using affibody-displaying BNCs. Cells were incubated with calcein-loaded Z_{HER2}-BNC-liposome complexes (Z_{HER2}-BNC/Lipo), Z_{WT}-BNC-liposome complexes (Z_{WT}-BNC/Lipo), or calcein-containing liposomes (Lipo) for 3 h. After three washes with serum-free medium, cells were recovered and assayed by flow cytometry. The RFL is given as the mean and standard deviation of three independent experiments. Closed bar: SK-BR-3; Open bar: MDA-MB-231.

formation. After gel filtration to remove non-incorporated calcein, freeze-dried Z_{HER2}-BNCs were added and incubated for 60 min to allow formation of the BNC-liposome complex. Large amount of calcein-containing liposome allowed that calcein was incorporated in almost all BNC-liposome complex. The complex was added to

SK-BR-3 or MBA-MB-231 cells (final concentration of proteins: 100 µg/ml) and incubated for 3 h. Then cells were washed and analyzed by flow cytometry (Fig. 5). High intensity calcein fluorescence was detected only from SK-BR-3 cells treated with Z_{HER2}-BNC/Lipo. Only minute fluorescence was observed from SK-BR-3 and MDA-MB-231 cells treated with Z_{WT}-BNC-liposome complexes (Z_{WT}-BNC/Lipo) or calcein-containing liposomes (Lipo) as negative controls.

In order to insure that calcein was internalized into the targeted cells, these cells were observed by laser-scanning confocal microscopy (Fig. 6). After 3 h incubation, calcein fluorescence was observed at the cell surface and cytoplasm of SK-BR-3 cells, which is similar to results obtained using anti-EGFR antibody displaying BNCs.[21] In the case of Z_{WT}-BNC/Lipo or Lipo to MDA-MB-231 used as target cells, no fluorescence was observed. These results suggest that Z_{HER2}-BNC/Lipo could transfer calcein into targeted cells efficiently and specifically.

In conclusion, a Z_{HER2}-affibody displayed BNC was developed for use as a HER2-targeted carrier. Z_{HER2}-BNC began binding to the SK-BR-3 cell surface after 30 min and SK-BR-3 cells bind the BNCs at a rate three times higher than MDA-MB-231 cells. The uptake signal of Z_{HER2}-BNC/LIP was about seven times higher than that of nude liposomes. This result demonstrates the ease with which it is possible to modify the liposome surface with high target specificity. In addition, affibody-displaying BNCs have stability in PBS almost as same as that of wild-type BNCs, which is also superior as a DDS carrier (data not shown). Our results indicate that the genetically engineered BNC we describe is a promising drug delivery carrier for cell-specific delivery.
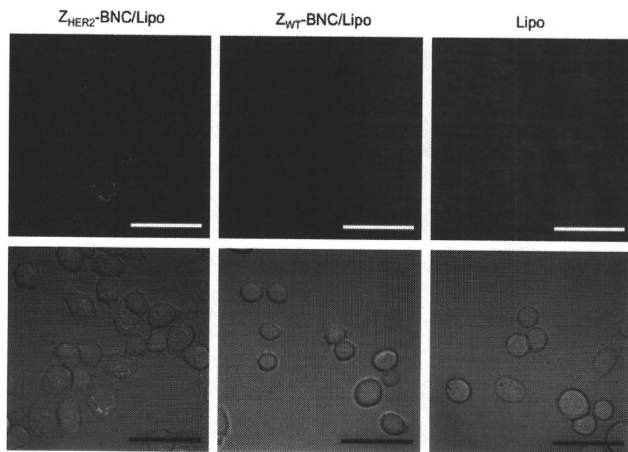
Acknowledgments

Figure 6. Fluorescence images of SK-BR-3 cells after treatment with calcein-loaded affibody-displaying BNCs. SK-BR-3 cells were incubated with calcein-loading Z_{HER2}-BNC/Lipo, Z_{WT}-BNC/Lipo, or Lipo for 3 h. After incubation, cells were washed three times with serum-free medium and then observed by laser-scanning confocal microscopy. Scale bar = 50 µm.

References and notes

1. Beuttler, J.; Rothdiener, M.; Muller, D.; Frejd, F. Y.; Kontermann, R. E. *Bioconjugate Chem.* **2009**, *20*, 1201.
2. Kirby, C.; Gregoriadis, G. *Nat. Biotechnol.* **1984**, *2*, 979.
3. Liu, S.; Maheshwari, R.; Kiick, K. L. *Macromolecules* **2009**, *42*, 3.
4. Kuroda, S.; Otaka, S.; Miyazaki, T.; Nakao, M.; Fujisawa, Y. *J. Biol. Chem.* **1992**, *267*, 1953.
5. Yamada, T.; Iwasaki, Y.; Tada, H.; Iwabuki, H.; Chuah, M. K.; VandenDriessche, T.; Fukuda, H.; Kondo, A.; Ueda, M.; Seno, M.; Tanizawa, K.; Kuroda, S. *Nat. Biotechnol.* **2003**, *21*, 885.
6. Iwasaki, Y.; Ueda, M.; Yamada, T.; Kondo, A.; Seno, M.; Tanizawa, K.; Kuroda, S.; Sakamoto, M.; Kitajima, M. *Cancer Gene Ther.* **2007**, *14*, 74.
7. Jung, J.; Matsuzaki, T.; Tatematsu, K.; Okajima, T.; Tanizawa, K.; Kuroda, S. *J. Controlled Release* **2008**, *126*, 255.
8. Shishido, T.; Yonezawa, D.; Iwata, K.; Tanaka, T.; Ogino, C.; Fukuda, H.; Kondo, A. *Bioorg. Med. Chem. Lett.* **2009**, *19*, 1473.
9. Nygren, P. A. *FEBS J.* **2008**, *275*, 2668.
10. Slamon, D. J.; Clark, G. M.; Wong, S. G.; Levin, W. J.; Ullrich, A.; McGuire, WL. *Science* **1987**, *235*, 177.
11. Witton, C. J.; Reeves, J. R.; Going, J. J.; Cooke, T. G.; Bartlett, J. M. *J. Pathol.* **2003**, *200*, 290.
12. Ross, J. S.; Fletcher, J. A. *Stem Cells* **1998**, *16*, 413.
13. Chen, J. S.; Lan, K.; Hung, M. C. *Drug Resist. Updat.* **2003**, *6*, 129.
14. Orlova, A.; Magnusson, M.; Eriksson, T. L.; Nilsson, M.; Larsson, B.; Hoiden-Guthenberg, I.; Widstrom, C.; Carlsson, J.; Tolmachev, V.; Stahl, S.; Nilsson, F. Y. *Cancer Res.* **2006**, *66*, 4339.
15. Tolmachev, V.; Orlova, A.; Pehrson, R.; Galli, J.; Baastrup, B.; Andersson, K.; Sandstrom, M.; Rosik, D.; Carlsson, J.; Lundqvist, H.; Wennborg, A.; Nilsson, F. Y. *Cancer Res.* **2007**, *67*, 2773.
16. Lee, S. B.; Hassan, M.; Fisher, R.; Chertov, O.; Chernomordik, V.; Kramer-Marek, G.; Gandjbakhche, A.; Capala, J. *Clin. Cancer Res.* **2008**, *14*, 3840.
17. Puri, A.; Kramer-Marek, G.; Campbell-Massa, R.; Yavlovich, A.; Tele, S. C.; Lee, S. B.; Clogston, J. D.; Patri, A. K.; Blumenthal, R.; Capala, J. *J. Liposome Res.* **2008**, *18*, 293.
18. Alexis, F.; Basto, P.; Levy-Nissenbaum, E.; Radovic-Moreno, A. F.; Zhang, L.; Pridgen, E.; Wang, A. Z.; Marein, S. L.; Westerhof, K.; Molnar, L. K.; Farokhzad, O. C. *ChemMedChem* **2008**, *3*, 1839.
19. Canine, B. F.; Wang, Y.; Hatefi, A. *J. Controlled Release* **2009**, *138*, 188.
20. Belousova, N.; Mikheeva, G.; Gelovani, J.; Krasnykh, V. *J. Virol.* **2008**, *82*, 630.
21. Kurata, N.; Shishido, T.; Muraoka, M.; Tanaka, T.; Ogino, C.; Fukuda, H.; Kondo, A. *J. Biochem.* **2008**, *144*, 701.
22. Yamada, T.; Iwabuki, H.; Kanno, T.; Tanaka, H.; Kawai, T.; Fukuda, H.; Kondo, A.; Seno, M.; Tanizawa, K.; Kuroda, S. *Vaccine* **2001**, *19*, 3154.
24. Orlova, A.; Tolmachev, V.; Pehrson, R.; Lindborg, M.; Tran, T.; Sandström, M.; Nilsson, F. Y.; Wennborg, A.; Abrahmsén, L.; Feldwisch, J. *Cancer Res.* **2007**, *67*, 2178.

Original Article

Clinical Results and Risk Factors of Proton and Carbon Ion Therapy for Hepatocellular Carcinoma

Shohei Komatsu, MD[1,2]; Takumi Fukumoto, MD, PhD[1]; Yusuke Demizu, MD, PhD[2]; Daisuke Miyawaki, MD, PhD[3];
Kazuki Terashima, MD[2]; Ryohei Sasaki, MD, PhD[3]; Yuichi Hori, MD, PhD[1]; Yoshio Hishikawa, MD, PhD[2];
Yonson Ku, MD, PhD[1]; and Masao Murakami, MD, PhD[2]

BACKGROUND: The objective of this study was to evaluate the clinical outcome of proton and carbon ion therapy for hepatocellular carcinoma (HCC). **METHODS:** In total, 343 consecutive patients with 386 tumors, including 242 patients (with 278 tumors) who received proton therapy and 101 patients (with 108 tumors) who received carbon ion therapy, were treated on 8 different protocols of proton therapy (52.8-84.0 gray equivalents [GyE] in 4-38 fractions) and on 4 different protocols of carbon ion therapy (52.8-76.0 GyE in 4-20 fractions). **RESULTS:** The 5-year local control and overall survival rates for all patients were 90.8% and 38.2%, respectively. Regarding proton and carbon ion therapy, the 5-year local control rates were 90.2% and 93%, respectively, and the 5-year overall survival rates were 38% and 36.3%, respectively. These rates did not differ significantly between the 2 therapies. Univariate analysis identified tumor size as an independent risk factor for local recurrence in proton therapy, carbon ion therapy, and in all patients. Multivariate analysis identified tumor size as the only independent risk factor for local recurrence in proton therapy and in all patients. Child-Pugh classification was the only independent risk factor for overall survival in proton therapy, in carbon ion therapy, and in all patients according to both univariate and multivariate analyses. No patients died of treatment-related toxicities. **CONCLUSIONS:** Proton and carbon ion therapies for HCC were comparable in terms of local control and overall survival rates. These therapies may represent innovative alternatives to conventional local therapies for HCC. *Cancer* 2011;00:000–000. © 2011 American Cancer Society.

KEYWORDS: hepatocellular carcinoma, particle therapy, proton therapy, carbon ion therapy, local recurrence.

Hepatocellular carcinoma (HCC) is the fifth leading cause of cancer death worldwide, and the majority of patients with HCC reside in Asian countries.[1,2] HCC is well suited to local therapy, because it has a tendency to stay within the liver, and distant metastasis generally occurs late. This implies that curative local therapy, as represented by hepatectomy and liver transplantation, has a great impact on the disease course and also offers the best chance of long-term survival for patients with HCC.[3,4] However, only 5% to 40% of patients with HCC are amenable to a hepatectomy because of either advanced tumors or coexisting cirrhosis,[5,6] and a shortage of liver grafts limits the applicability of liver transplantation. Although local ablative therapies, such as radiofrequency ablation (RFA), recently have gained widespread clinical acceptance, there is growing evidence of a high local recurrence rate after RFA that reaches up to 36%.[7,8] In addition, local ablative therapies also are unsuitable for patients who have bleeding tendencies, unfavorable anatomic tumor locations, or large tumors.[8,9] Patients who are not eligible for local ablative therapies usually receive noncurative modalities, such as transarterial chemoembolization (TACE) or systemic chemotherapy.

Radiotherapy also is a local therapy but historically has played a limited role in the treatment of HCC, because the hepatic tolerance dose is lower than the tumoricidal dose, especially when liver function is impaired by chronic liver disease.[10-12] Particle beams, such as proton and carbon ion beams, have demonstrated an increase in energy deposition with a penetration depth up to a sharp maximum at the end of their range: the so-called Bragg peak phenomenon.[13] Therefore, higher tumor doses can be delivered without increasing toxicity to the surrounding noncancerous tissues and organs. Particle therapy results for HCC have been reported in several case series, all of which have reported good overall survival and encouraging local control rates.[14-19] However, most of those studies were conducted at proton treatment centers, and few

Table 1. Patient Characteristics

Characteristic	No. of Patients (%)		
	Proton Therapy, n=242	Carbon Ion Therapy, n=101	All Patients, n=343
Age, y			
<70	115 (48)	55 (54)	170 (50)
≥70	127 (52)	46 (46)	173 (50)
Sex			
Men	182 (75)	73 (72)	255 (74)
Women	60 (25)	28 (28)	88 (26)
Positive viral marker			
Hepatitis B virus	27 (11)	19 (19)	46 (13)
Hepatitis C virus	159 (66)	60 (59)	219 (64)
None	54 (22)	21 (21)	75 (22)
Both	2 (1)	1 (1)	3 (1)
Performance status			
0	172 (71)	73 (72)	245 (71)
1	57 (24)	18 (18)	75 (22)
2	10 (4)	9 (9)	19 (6)
3	3 (1)	1 (1)	4 (1)
Child-Pugh classification			
A	184 (76)	78 (77)	262 (76)
B	55 (23)	20 (20)	75 (22)
C	3 (1)	3 (3)	6 (2)
BCLC stage			
0	9 (4)	9 (9)	18 (5)
A	82 (34)	36 (36)	118 (34)
B	32 (13)	15 (15)	47 (14)
C	113 (47)	37 (36)	150 (44)
D	6 (2)	4 (4)	10 (3)
Recommended treatment according to BCLC stage			
Resection: Operable group	49 (20)	29 (29)	78 (23)
Others: Inoperable group	193 (80)	72 (71)	265 (77)
No. of tumors			
Single	213 (88)	81 (80)	294 (86)
Multiple	29 (12)	20 (20)	49 (14)

Abbreviations: BCLC, Barcelona Clinic Liver Cancer.

studies have reported results of carbon ion therapy for HCC. To our knowledge, no reports have focused on the differences in treatment results between the 2 types of particle beams.

The Hyogo Ion Beam Medical Center (HIBMC) is the only facility in the world that provides both proton and carbon ion therapies.[20] In the current study, we analyzed the efficacy and safety of proton and carbon ion therapy for HCC at the HIBMC.

MATERIALS AND METHODS

Patient and Tumor Characteristics

The current study was conducted according to the Helsinki Declaration, and written informed consent was obtained from all patients. From May 2001 to January 2009, 343 consecutive patients with 400 HCCs were treated at the HIBMC (excluding 6 patients who discontinued treatment). Patients who met the following conditions were ineligible for treatment: 1) uncontrolled ascites and 2) tumors that measured >15 cm in greatest dimension (the upper limit of the irradiation field). No patients were lost to follow-up, although we could not evaluate the post-treatment imaging findings from 12 patients with 14 tumors. Thus, overall survival rates were determined for all 343 patients, and local control rates were determined for 386 tumors. In total, 242 patients with 278 tumors received proton therapy, and 101 patients with 108 tumors received carbon ion therapy. For all patients,

Table 2. Tumor Characteristics

Characteristic	No. of Tumors (%)		
	Proton Therapy, n=278	Carbon Ion Therapy, n=108	All Patients, n=386
Tumor size, mm			
<50	196 (71)	81 (75)	277 (72)
50-100	65 (23)	22 (20)	87 (22)
>100	17 (6)	5 (5)	22 (6)
Gross classification			
Single nodular type	153 (55)	54 (50)	207 (53)
Single nodular with extranodular growth type	85 (30)	41 (38)	126 (33)
Confluent multinodular type	13 (5)	6 (6)	19 (5)
Infiltrative type	27 (10)	7 (6)	34 (9)
Macroscopic vascular invasion			
Yes	73 (26)	19 (18)	92 (24)
No	205 (74)	89 (82)	294 (76)
Perivascular location			
Yes	121 (44)	32 (30)	153 (40)
No	157 (56)	76 (70)	233 (60)
Prior treatment history to the target tumor			
Yes	132 (47)	49 (45)	181 (47)
No	146 (53)	59 (55)	205 (53)
Serum AFP, ng/mL			
<100	184 (66)	72 (67)	256 (66)
≥100	94 (34)	36 (33)	130 (34)
Serum PIVKAII, mAU/mL			
<100	129 (46)	58 (54)	187 (48)
≥100	149 (54)	50 (46)	199 (52)

Abbreviations: AFP, α-fetoprotein; PIVKAII, protein induced by vitamin K absence or antagonist II.

HCC was diagnosed on the basis of the results from imaging studies, which usually included a combination of contrast-enhanced computed tomography (CT) and magnetic resonance imaging (MRI) studies. Tumor markers, including serum α-fetoprotein (AFP) and serum protein induced by vitamin K absence or antagonist II (PIVKAII), also were measured before and after treatment. Chest CT scans, bone scintigrams, and positron-emission tomography studies, if necessary, were obtained to exclude the possibility of distant metastasis.

Patient and tumor characteristics are summarized in Tables 1 and 2, respectively, for the proton and carbon ion therapy groups and for all patients. All the patients were staged and categorized as either operable (operable group) or inoperable (inoperable group) according to Barcelona Clinic Liver Cancer (BCLC) classification criteria.[21] Tumors were classified into 3 groups according to tumor size (<50 mm, 50-100 mm, and >100 mm). All tumors were divided grossly into 4 types according to Liver Cancer Study Group of Japan criteria[22]: 1) single

nodular type, 2) single nodular type with extranodular growth, 3) confluent multinodular type, and 4) infiltrative type. Studies have indicated that single nodular type tumors have a better prognosis than the other tumor types;[23] therefore, all tumors were categorized further as either single nodular type or nonsingle nodular type. Macroscopic vascular invasion was defined as gross tumor vascular invasion into the portal or hepatic veins identified by pretreatment imaging. Perivascular location was defined as a situation in which the tumor invaded or abutted the main portal trunk and/or inferior vena cava. Among the 181 tumors that had received treatment before particle therapy, 2 tumors were classified as local recurrences after hepatectomy, and 60 tumors were classified as local recurrences after percutaneous local therapy. In addition, 169 target tumors had undergone TACE before particle therapy. All data were analyzed retrospectively for proton and carbon ion therapy, and all patients were considered with regard to local tumor control rates, overall patient survival rates, and treatment-related toxicities.

Table 3. Treatment Protocols

BED$_{10}$[a]	Protocol (BED$_{10}$)	No. of Patients [%]
Proton therapy		
<100	76 GyE/38 Fr (91.2)	11 [4]
	56 GyE/8 Fr (95.2)	4 [2]
	60 GyE/10 Fr (96.0)	89 [37]
≥100	76 GyE/20 Fr (104.88)	70 [29]
	66 GyE/10 Fr (109.56)	53 [22]
	80 GyE/20 Fr (112)	3 [1]
	84 GyE/20 Fr (119.28)	3 [1]
	52.8 GyE/4 Fr (122.496)	9 [4]
Carbon ion therapy		
<100	52.8 GyE/8 Fr (87.648)	23 [23]
≥100	76 GyE/20 Fr (104.88)	3 [3]
	66 GyE/10 Fr (109.56)	16 [16]
	52.8 GyE/4 Fr (122.496)	59 [58]

Abbreviations: BED$_{10}$, biologic effective dose for acute-reacting tissues; Fr, fractions; GyE, gray equivalents.
[a] The BED$_{10}$ was calculated by linear-quadratic formalism assuming an α/β ratio of 10 GyE.

Treatment Protocol

The biologic effects of both proton and carbon ion therapy at the HIBMC were evaluated in vitro and in vivo, and the relative biologic effectiveness (RBE) values of these therapies were determined as 1.1 and 2,0 to 3.7, respectively (depending on the depth of the spread-out Bragg peaks).[24] Because we assumed that all tissues had almost the same RBE for protons or carbon ions, doses expressed in gray equivalents (GyE), were directly comparable to photon doses.

Eight protocols for proton therapy (52.8-84 GyE in 4-38 fractions using 150-megaelectron volt [MeV], 190-MeV, 210-MeV, or 230-MeV proton beams) and 4 protocols for carbon ion therapy (52.8-76 GyE in 4-20 fractions using 250-MeV or 320-MeV carbon ion beams) were used during the study period (Table 3). The radiobiologic equivalent dose for acute-reacting tissues (BED$_{10}$) was calculated for each protocol. The protocols for proton and carbon ion therapy were set first on the basis of earlier experience at the National Cancer Center East (Kashiwa, Japan), the Proton Medical Research Center (Tsukuba, Japan), and the National Institute of Radiological Sciences (Chiba, Japan). Thereafter, we adopted dose-escalation or hypofractionation protocols, depending on patient and tumor factors.

The policy for the selection of beam type was determined by the following: 1) from May to October 2001 and from April 2003 to March 2005, only proton therapy was available (52 patients with 57 tumors); 2) from Feb-ruary to June 2002, only carbon ion therapy was available (6 patients with 6 tumors); and 3) since April 2005, treatment plans for both proton and carbon ion therapy were made for all patients, and a better suited beam was selected on the basis of the treatment plans (285 patients with 323 tumors). Regarding the choice of either proton beam or carbon ion beam therapy, the following factors were considered: 1) the values for the percentage prescription dose received by at least 95% volume (D95) of the gross tumor volume (GTV), 2) D95 of the clinical target volume (CTV), 3) D95 of the planning target volume (PTV), 4) the percentage of the volumes of hepatic noncancerous portions (entire liver volume − GTV) receiving ≥30 GyE (Liver V30), 5) the maximum exposure doses of the adjacent gut (Gut Dmax), 6) the percentage of the volumes of the adjacent gut receiving ≥40 GyE (Gut V40), 7) the maximum exposure doses to the skin, and 8) the maximum exposure doses to the ribs. D95 of the PTV and Liver V30 values have always been high-priority factors. Among these factors, Liver V30 is used as the most important factor for patients whose liver function already has deteriorated, and Gut Dmax and/or Gut V40 values have become secondary major concerning factors in patients who have tumors located close to the gut.

A representative case presentation of treatment plans for both proton therapy and carbon ion therapy is provided in Figure 1. The D95 of PTV was equal for proton and carbon ion therapy. Conversely, Gut Dmax and Gut V40 were significantly higher for the proton treatment plan than for the carbon ion treatment plan. Therefore, carbon ion therapy was selected in this representative case.

Treatment Planning

The radiation treatments were designed to use a CT-based, 3-dimensional treatment planning system (FOCUS-M; CMS, Tokyo, Japan; and Mitsubishi Electric, Kobe, Japan). CT images were obtained at the phase of expiration using a respiratory gating system. A respiratory gating irradiation system that was developed at the National Institute of Radiological Sciences in Chiba[25] was used for irradiation of the beam during the exhalation phase for all patients. The GTV and the organs at a risk of irradiation, such as the liver and intestines, were delineated according to fusion images that were constructed from contrast-enhanced CT and MRI studies. Treatment planning was defined as follows: CTV = GTV + 5 mm, PTV = CTV + 5 mm. In addition, another 5-mm to 10-mm margin was included in the caudal axis to compensate for uncertainty caused by respiration-induced
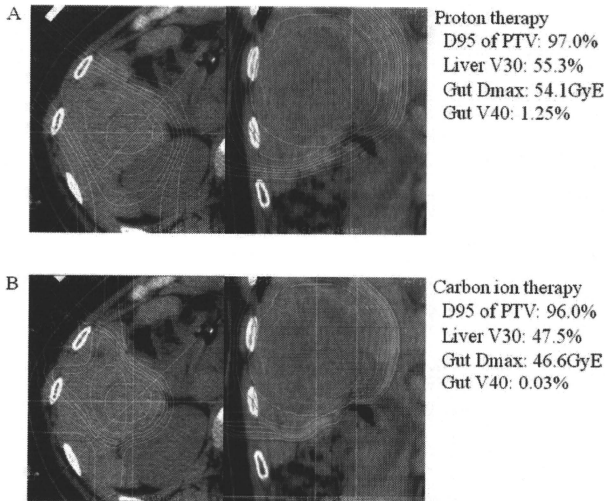
A

Proton therapy
D95 of PTV: 97.0%
Liver V30: 55.3%
Gut Dmax: 54.1GyE
Gut V40: 1.25%

B

Carbon ion therapy
D95 of PTV: 96.0%
Liver V30: 47.5%
Gut Dmax: 46.6GyE
Gut V40: 0.03%

Figure 1. These images are from a representative case presentation of treatment plans for both (A) proton therapy and (B) carbon ion therapy. D95 indicates the dose received by at least 95% volume; PTV, planning target volume; Liver V30, percentage volumes of noncancerous hepatic portions (entire liver volume − gross tumor volume) that received ≥30 gray equivalents (GyE); Gut Dmax, the maximum exposure doses of the adjacent gut; Gut V40, percentage volumes of the adjacent gut that received ≥40 GyE.

hepatic movements. Doses were calculated on the basis of the pencil beam algorithm. Beam parameters, including energy level, the width of the spread-out Bragg peak, and degrader thickness, were selected adequately using FOCUS-M. Dose-volume histograms were calculated for all patients to evaluate the risk of radiation-induced liver disease.

Follow-Up and Evaluation Criteria

Patients underwent a complete blood count, biochemical profile, detection of tumor markers (including serum AFP and PIVKAII), and abdominal imaging studies (CT or MRI) every 3 months for 3 years after treatment and every 6 months thereafter. In general, for patients with HCC, the objective of all effective locoregional therapies is to obtain necrosis of the tumor regardless of the shrinkage of the lesion. Even if extensive tumor necrosis is achieved, this may not be accompanied by a reduction in the greatest dimension of the lesion. Consequently, several studies have indicated that World Health Organization and

Response Evaluation Criteria in Solid Tumors criteria have no value in the assessment of tumor response after locoregional therapies in patients with HCC.[26,27] It has been reported that such tumors, even after complete response, tend to persist for a long period after the completion of particle therapy.[19] Therefore, local recurrence was defined either as the growth of an irradiated tumor or as the appearance of new tumors within the PTV based on criteria established in previous reports.[16,17,19,28] Acute and late toxicities were graded according to the National Cancer Institute Common Terminology Criteria for Adverse Events (version 2.0; National Cancer Institute, Bethesda, Md).

Statistical Analyses

The statistical significance of differences in each classification for both local control and overall survival rates was estimated by the Kaplan-Meier method and was compared using the log-rank test. Univariate and multivariate analyses using Cox proportional hazards regression
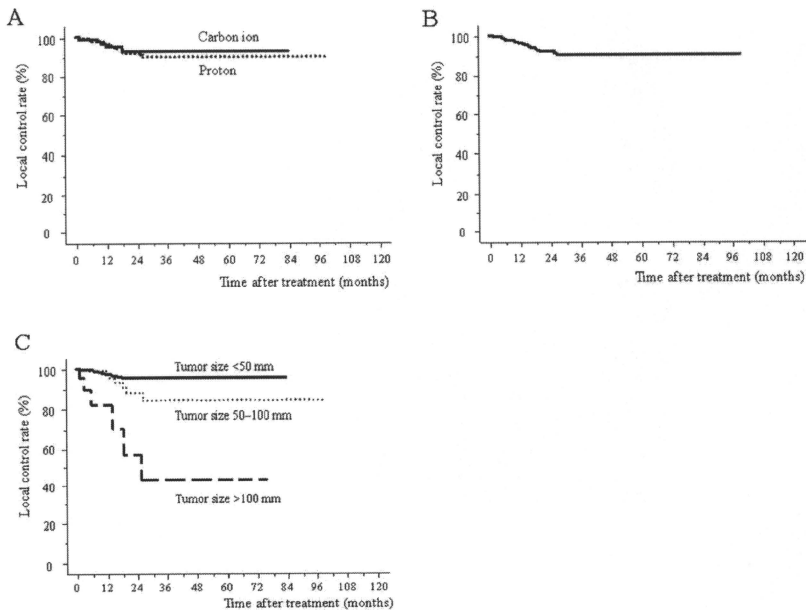
Figure 2. Local control rates after treatment are illustrated for (A) tumors that were treated with proton and carbon ion therapy, (B) all 386 tumors, and (C) all 386 tumors according to tumor size.

models were used to identify independent risk factors that predicted local control and overall survival rates. Differences of $P < .05$ were considered statistically significant, and variables with $P < .10$ were entered into a multivariate analysis using a Cox proportional hazards model. All statistical analyses were performed using SPSS statistical software (version 17.0 for Windows; SPSS, Inc., Chicago, Ill).

RESULTS

Local Control Rates After Proton and Carbon Ion Therapies

Patients were followed either until death or to March 2010 (median follow-up, 31.0 months). Among 343 patients with 386 tumors, 223 patients developed recurrences after treatment. Nineteen patients developed extra-

hepatic metastasis, and 210 patients developed intrahepatic recurrences, including 23 local recurrences (proton therapy, 18 patients; carbon ion therapy, 5 patients). The longest interval to local recurrence was 27.1 months, and all local recurrences developed within 3 years. The 5-year local control rates for patients who received proton therapy and carbon ion therapy were 90.2% and 93%, respectively (Fig. 2A). The effective 3-year and 5-year local control rates for all 386 tumors were both 90.8% (Fig. 2B). An analysis of the local control rates according to the tumor factors identified above (see Treatment Protocols) is listed in Table 4. Univariate analysis revealed that tumor size was a significant risk factor for local recurrence in the proton therapy group, the carbon ion therapy group, and all patients. In multivariate analysis, tumor size was identified as an independent risk factor for local recurrence in the proton therapy group

Cancer   Month 00, 2011

Table 4. Univariate Analysis of Prognostic Factors for Local Control Rate

Factor	Proton Therapy, n=278		Carbon Ion Therapy, n=108		All Patients, n=386	
	LC Rate at 5 Years, %	P	LC Rate at 5 Years, %	P	LC Rate at 5 Years, %	P
Tumor size, mm		<.0001		.0062		<.0001
<50	95.5		94.5		95.3	
50-100	84.1		90.9		84.4	
>100	43.4		80		42.2	
Gross classification		.0901		.0943		.0219
Single nodular type	93.3		96		94	
Nonsingle nodular type	86.2		89.4		86.7	
Macroscopic vascular invasion		.2544		.0292		.0535
Yes	83.9		80.4		82.8	
No	92		94.8		92.8	
Perivascular location		.0704		.4267		.0403
Yes	85.5		86.8		85.7	
No	93.5		95.1		93.8	
Prior treatment history		.7332		.9000		.7629
Yes	91.5		95		92	
No	89.2		91.9		89.9	
Serum AFP, ng/mL		.5352		.6111		.4310
<100	90.9		95.1		91.8	
≥100	89		86.8		88.6	
Serum PIVKAII, mAU/mL		.0997		.3468		.2976
<100	94.5		90.1		93.4	
≥100	85.5		97.9		87.8	

Abbreviations: AFP, α-fetoprotein; LC, local control; PIVKAII, protein induced by vitamin K absence or antagonist II.

and in all patients (Table 5). In addition, the local control rates for all 386 tumors that measured <50 mm, 50 to 100 mm, and >100 mm were 95.3%, 84.4%, and 42.2%, respectively (Fig. 2C). In contrast, other tumor factors, including gross classification, macroscopic vascular invasion, perivascular location, treatment history, serum AFP level, and serum PIVKAII level, did not affect the local control rate in any tumor subset in multivariate analysis.

Overall Survival Rates of Proton and Carbon Ion Therapies

The 5-year overall survival rates for patients who received proton therapy and carbon ion therapy were 38% and 36.3%, respectively (Fig. 3A). The overall survival rates for all 343 patients at 3 years and 5 years were 59% and 38.2%, respectively (Fig. 3B). Univariate and multivariate analyses of the overall survival rates according to the 8 relevant tumor factors are provided in Tables 6 and 7, respectively. According to the univariate analysis, Child-Pugh classification, macroscopic vascular invasion, and serum AFP levels were the only factors that significantly affected the overall survival rates in all groups (proton

therapy, carbon ion therapy, and all patients) (Table 6). The Child-Pugh classification was the only independent factor for overall survival in proton therapy, carbon ion therapy, and all patients according to the multivariate analysis (Table 7). The 5-year overall survival rates for Child-Pugh classifications A, B, and C were 46.6%, 8.7%, and 0%, respectively (Fig. 3C).

The 5-year overall survival rates for BCLC stages 0, A, B, C, and D were 80.8%, 52.7%, 23.7%, 30.6%, and 0%, respectively (Fig. 4A). According to the BCLC classification, hepatic resection was categorized as stage 0 and part of stage A. In total, 78 patients were categorized into the hepatic resection group. The 5-year overall survival rates for patients classified into groups according to whether they underwent hepatic resection (operable group) or received treatments (inoperable group) were 67.6% and 29.4%, respectively (P < .0001) (Fig. 4B).

Local Control and Overall Survival Rates According to the BED$_{10}$

We also analyzed the local control and overall survival rates after both proton and carbon ion therapies according

Table 5. Independent Risk Factors Related to the Local Control Rate: Multivariate Analysis

Factor	SE	Chi-Square Statistic	RR	95% CI	P
Proton therapy					
Tumor size, mm					.0030
50-100 (vs <50)	0.666	1.175	2.058	0.558-7.590	
>100 (vs <50)	0.703	10.463	9.725	2.450-38.596	
Single nodular type (vs nonsingle nodular type)	0.538	0.187	1.262	0.440-3.623	.6652
Perivascular location: Yes (vs no)	0.543	0.147	0.812	0.280-2.354	.7011
Serum PIVKAII ≥100 mAU/mL (vs <100 mAU/mL)	0.530	0.389	1.392	0.492-3.937	.5327
Carbon ion therapy					
Tumor size, mm					.4703
50-100 (vs <50)	1.569	0.069	0.662	0.031-14.322	
>100 (vs <50)	1.905	0.575	4.239	0.101-177.314	
Single nodular type (vs nonsingle nodular type)	1.231	1.110	3.658	0.328-40.853	.2921
Macroscopic vascular invasion: Yes (vs no)	1.585	0.347	2.544	0.114-56.848	.5557
All patients					
Tumor size, mm					.0002
50-100 (vs <50)	0.646	10.527	8.122	2.291-28.789	
>100 (vs <50)	0.562	2.146	0.439	0.146-1.321	
Single nodular type (vs nonsingle nodular type)	0.519	2.544	2.288	0.827-6.327	.1107
Macroscopic vascular invasion: Yes (vs no)	0.651	2.601	2.860	0.798-10.253	.1068
Perivascular location: Yes (vs no)	0.506	0.738	0.647	0.240-1.745	.3902

Abbreviations: CI, confidence interval; PIVKAII, protein induced by vitamin K absence or antagonist II; RR, relative risk; SE, standard error.

to the BED_{10} using a cutoff score of 100 (Fig. 5). The 5-year local control rates for tumors that were treated on the protocols characterized by BED_{10} values <100 and ≥100 were 93.3% and 87.4%, respectively, for proton therapy and 80.7% and 95.7%, respectively, for carbon ion therapy. The 5-year overall survival rates for patients who were treated on the protocols characterized by BED_{10} values <100 and ≥100 were 31.7% and 43.9%, respectively, for proton therapy and 32.3% and 48.4%, respectively, for carbon ion therapy. There was no significant difference in local control and overall survival rates, irrespective of the BED_{10} score, between proton therapy and carbon ion therapy.

Toxicities

All acute toxicities that occurred during treatment were transient, easily managed, and acceptable. However, grade ≥3 late toxicities were observed in 8 patients on proton therapy and in 4 patients on carbon ion therapy, and 4 of 12 patients were diagnosed with radiation-induced liver disease (Table 8). However, all of these patients with hematologic disorders were asymptomatic and required no further treatment. In addition, upper gastrointestinal ulcer, pneumonitis, and subcutaneous panniculitis healed with conservative management. Five patients who received proton therapy developed refractory skin ulcers,

and 1 patient required skin transplantation. A salvage drainage operation also was required by 1 patient who developed infectious biloma 10 months after irradiation. No patients died of treatment-related toxicity.

DISCUSSION

We analyzed the safety and efficacy of particle therapy using proton and carbon ion beams for HCC in a single center. The key findings of this study are as follows: 1) particle therapy produced excellent local control and overall survival rates with acceptable adverse events, 2) the treatment results from carbon ion therapy appeared to be equivalent to those from proton therapy, and 3) tumor size was the only risk factor that affected the local control rate.

Local control rates for both proton therapy and carbon ion therapy exceeded 90% in the current study. These data are very similar to those related to particle therapy for HCC, whereas they are superior to data related to conformal radiotherapy.[16,18,29,30] Recent improvements in dose localization techniques, such as intensity-modulated radiotherapy, conformal 3-dimensional planning, and breathing motion management strategies, thus, have made it possible to irradiate smaller, well defined targets in the liver. However, these highly computer-assisted
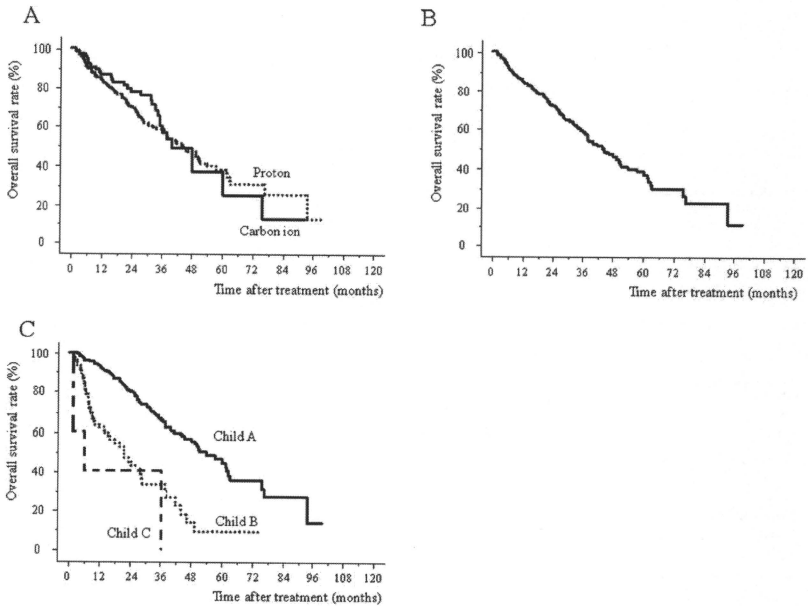
A

B

C

Figure 3. Overall survival rates after treatment are illustrated for (A) patients who received with proton and carbon ion therapy, (B) all 343 patients, and (C) all 343 patients according to Child-Pugh classification.

irradiation techniques using photon beams have achieved limited efficacy in treating patients with HCC. The local control rates produced by these conformal approaches remain in the 40% to 66% range for several reasons.[29,30] Radiation-induced liver disease still is observed frequently with conformal approaches when a sufficient dose is delivered to completely kill the cells of the entire tumor nodule. This is especially the true for large and centrally situated liver tumors.[31] In this regard, particle beams can achieve an excellent dose distribution to these targets. The area of radiation dose deposition can be controlled well by the beam energy, because there is a rapid drop-off in energy deposition beyond the target area. Indeed, such theoretical advantages of particle therapy were proven in part by the impressively high local control rate of approximately 90% in the current study. Therefore, we believe that it is reasonable to say that the tumor-eliminating

capability of particle therapy is closely equivalent to that of hepatectomy, an outcome that has not been achieved with other radiation therapies.

Experience in the treatment of HCC by particle therapy has been accumulated mainly in Japanese centers, but there is increasing interest in other countries as well. There were 26 active proton therapy facilities as of February 2009, whereas there were only 3 carbon ion therapy facilities.[32] Until now, several proton treatment centers and 1 carbon ion treatment center have reported HCC treatments results.[16-19] However, except for the HIBMC, no single facility can deliver both proton and carbon ion beams. Therefore, our facility has a distinct advantage over other institutes with regard to comparing the efficacy of the 2 beams. To select proton therapy or carbon ion therapy, we made treatment plans for both proton and carbon ion therapy. When dose distributions were

Table 6. Univariate Analysis of Prognostic Factors for Overall Survival Rate

Factor	Proton Therapy, n=242		Carbon Ion Therapy, n=101		All Patients, n=343	
	OS Rate at 5 Years, %	P	OS Rate at 5 Years, %	P	OS Rate at 5 Years, %	P
Age, y		.7986		.6769		.6448
<70	37.3		43.9		39.4	
≥70	38.2		26.9		36.2	
Positive viral marker		.9754		.1805		.8586
Hepatitis B virus	34.9		44.6		32.4	
Hepatitis C virus	35.8		40.8		36.3	
None	46.7		33.9		46.6	
Performance status		<.0001		.2295		<.0001
0	43.5		43.7		43.6	
1 or 2 or 3	24.8		26.8		24.1	
Child-Pugh classification		<.0001		<.0001		<.0001
A	46.8		41.2		46.6	
B or C	8.2		33.3		8	
Tumor size, mm		.1438		.0003		.0038
<50	37.8		53.5		39.2	
50-100	37.4		17.9		33.8	
>100	41.1		0		39.8	
Macroscopic vascular invasion		.0003		.0055		<.0001
Yes	33.2		22		31.5	
No	40.3		47.8		40.2	
Serum AFP, ng/mL		.0026		.0024		<.0001
<100	42		30.9		42.6	
≥100	29.5		23.1		28.9	
Serum PIVKAII, mAU/mL		.0109		.4041		.0082
<100	40.4		58.4		41.8	
≥100	35.5		16.5		33.8	

Abbreviations: AFP, α-fetoprotein; OS, overall survival; PIVKAII, protein induced by vitamin K absence or antagonist II.

compared, there were many instances in which low-dose areas had spread into the surrounding normal liver during proton therapy planning. This was apparently because of the relatively large penumbra of proton beams. Consequently, dose distribution in a single beam appears to be better in carbon ion therapy than in proton therapy. However, in terms of beam arrangement, carbon ions are emitted from 3 fixed ports, such as vertical, horizontal, or 45-degree oblique; whereas a 360-degree rotating gantry can be used for protons. The high positioning accuracy achieved by irradiating patients in a supine position also was an advantage of proton therapy. Currently, 360-degree rotating gantries for carbon ion beams are under construction in Japan and Germany, and it is expected that these will enable the delivery of highly precise carbon ion beam arrangements and, thus, will improve the effectiveness of carbon ion therapy for HCC.

In addition to dose distribution, there are evident differences in biologic properties between the 2 beams, ie, the RBE. The RBE for proton therapy is comparatively simple. The International Commission on Radiation Units and Measurements has recommended 1.1 as a generic RBE for proton therapy based on an analysis of the published RBE values determined from in vivo systems.[33,34] All proton therapy centers, including the HIBMC, have accepted this recommendation. Conversely, the RBE for carbon ion therapy is complex, because there is no common model for selecting the RBE of carbon ion beams. In addition, it may vary depending on tissue type and the depth of the spread-out Bragg peaks.[32] Because of these differences, planning the physical dose distribution is substantially more complex for carbon ion beams than for proton beams; therefore, a direct comparison of proton therapy and carbon ion therapy is

Table 7. Independent Risk Factors Related to the Overall Survival Rate: Multivariate Analysis

Factor	SE	Chi-Square Statistic	RR	95% CI	P
Proton therapy					
Performance status 1-3 (vs 0)	0.200	9.283	0.544	0.368-0.805	.0023
Child-Pugh classification B or C (vs A)	0.204	29.731	0.329	0.220-0.490	<.0001
Macroscopic vascular invasion: Yes (vs no)	0.203	9.410	0.536	0.360-0.799	.0022
Serum AFP ≥100 ng/mL (vs <100 ng/mL)	0.198	2.281	1.349	0.915-1.990	.1310
Serum PIVKAII ≥100 mAU/mL (vs <100 mAU/mL)	0.199	1.231	1.248	0.844-1.844	.2672
Carbon ion therapy					
Child-Pugh classification B or C (vs A)	0.519	17.642	0.113	0.041-0.313	<.0001
Tumor size, mm					.0297
50-100 (vs <50)	0.569	6.795	4.412	1.445-13.468	
>100 (vs <50)	1.040	3.217	6.454	0.841-49.524	
Macroscopic vascular invasion: Yes (vs no)	0.625	0.647	1.654	0.486-5.631	.4211
Serum AFP ≥100 ng/mL (vs <100 ng/mL)	0.396	5.406	2.513	1.156-5.465	.0201
All patients					
Performance status 1-3 (vs 0)	0.180	10.852	0.554	0.389-0.787	.0010
Child-Pugh classification B or C (vs A)	0.182	45.663	0.292	0.204-0.417	<.0001
Tumor size, mm					.5976
50-100 (vs <50)	0.220	0.044	1.047	0.680-1.613	
>100 (vs <50)	0.375	0.656	0.738	0.354-1.539	
Macroscopic vascular invasion: Yes (vs no)	0.216	10.960	0.489	0.320-0.747	.0009
Serum AFP ≥100 ng/mL (vs <100 ng/mL)	0.176	4.848	1.474	1.044-2.083	.0277
Serum PIVKAII ≥100 mAU/mL (vs <100 mAU/mL)	0.186	0.922	1.196	0.830-1.724	.3371

Abbreviations: AFP, α-fetoprotein; CI, confidence interval; PIVKAII, protein induced by vitamin K absence or antagonist II; RR, relative risk; SE, standard error.
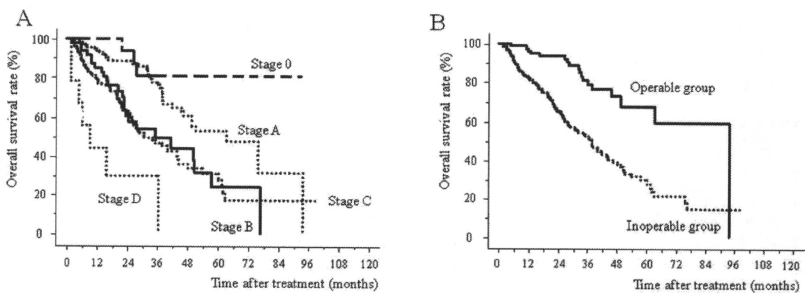

Figure 4. (A) Overall survival rates are illustrated for all 343 patients according to disease stage classified by the Barcelona Clinic Liver Cancer classification. (B) Overall survival rates are illustrated for all 343 patients according to the operative indication based on the Barcelona Clinic Liver Cancer classification.

not feasible. Under these circumstances, we established that the treatment results of carbon ion therapy were equivalent to those of proton therapy at our institute. These results may prove the validity of our treatment planning system for carbon ion therapy by using a variable RBE.

The current study has established the equal effectiveness of proton and carbon ion therapies for HCC. With regard to this result, we speculate that the superior dose

distribution compensates for the limitation of carbon ion beam arrangements at HIBMC. With the development of irradiation equipment, compared with proton therapy, carbon ion therapy will play a major role in the treatment of patients with HCC who have tumors adjacent to the gut and/or those whose liver function has deteriorated. However, carbon ion therapy requires huge economic resources, and this issue should be resolved in the future.
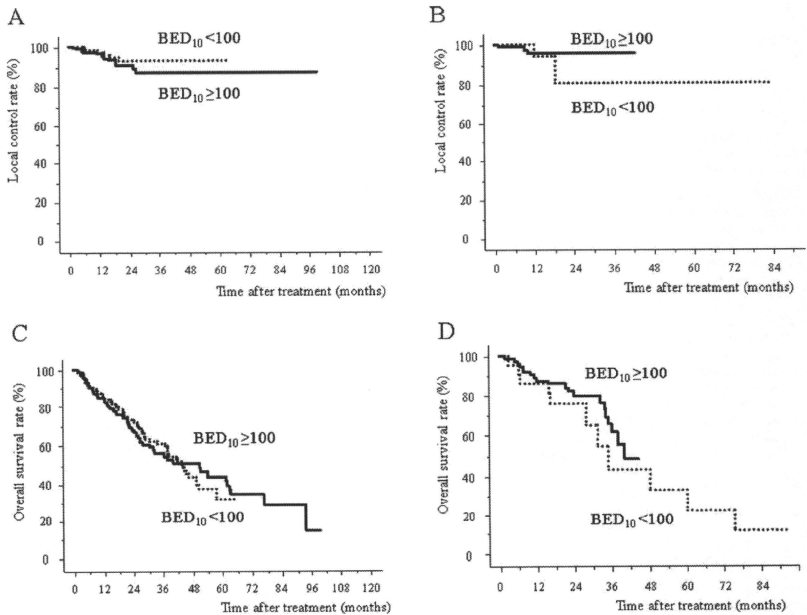
Figure 5. Local control rates are illustrated according to the radiobiologic equivalent dose for acute-reacting tissues (BED_{10}) for (A) proton therapy and (B) carbon ion therapy. Overall survival rates are illustrated according to the BED_{10} for (C) proton therapy and (D) carbon ion therapy.

Tumor size was the only significant risk factor for local recurrence after particle therapy (for proton therapy, carbon ion therapy, and all patients). Conversely, it is noteworthy that the 6 other tumor factors, including gross classification, macroscopic vascular invasion, perivascular location, prior treatment history, serum AFP levels, and serum PIVKAII levels, had no significant influence on the local control rate after either therapy. The application of local ablative therapies is contraindicated in tumors with vascular invasion,[9,35] and it has been reported by several studies that perivascular location significantly increased the local recurrence rate after RFA mainly because of the heat-sink effect.[8,9] In addition, hepatectomy frequently is abandoned to as a treatment for centrally situated tumors adjacent to the inferior vena cava and/or the main portal trunk in patients with cirrhosis, because these tumor loca-

tions tend to require major hepatectomy. In the current study, however, neither factor reduced the efficacy of proton therapy or carbon ion therapy in terms of the local control rate.

The local control rates achieved with proton therapy and carbon ion therapy for tumors <50 mm were 95.5%, and 94.5%, respectively. These data are similar or superior to those reported with local ablative therapies.[36] At the same time, the local control rates achieved with proton therapy and carbon ion therapy for tumors that measured from 50 mm to 100 mm in greatest dimension were 84.1% and 90.9%, respectively (Table 4). Because the upper limit of tumor size is 50 mm for local ablative therapies, these results clearly demonstrate the distinct advantage of particle therapy over other local therapies for tumors ≥50 mm. Taken together, in our opinion, particle

Table 8. Late Toxicities After Proton and Carbon Ion Therapy

No. of Patients (%)

Toxicity	Grade 2			Grade 3			Grade 4		
	Proton Therapy	Carbon Ion Therapy	All Patients	Proton Therapy	Carbon Ion Therapy	All Patients	Proton Therapy	Carbon Ion Therapy	All Patients
Dermatitis	12 (5)	5 (5)	17 (5)	4 (2)	0	4 (1)	1 (1)	0 (0)	1 (1)
Elevation of transaminase level	5 (2)	3 (3)	8 (2)	1 (1)	3 (3)	4 (1)	0 (0)	0 (0)	0 (0)
Upper gastrointestinal ulcer	3 (1)	1 (1)	4 (1)	1 (1)	0 (0)	1 (1)	0 (0)	0 (0)	0 (0)
Rib fracture	8 (3)	3 (3)	11 (3)	0 (0)	0 (0)	0 (0)	0 (0)	0 (0)	0 (0)
Pneumonitis	4 (2)	2 (2)	6 (2)	0 (0)	0 (0)	0 (0)	0 (0)	0 (0)	0 (0)
Subcutaneous panniculitis	6 (2)	2 (2)	8 (2)	0 (0)	1 (1)	1 (1)	0 (0)	0 (0)	0 (0)
Biloma	0 (0)	0 (0)	0 (0)	1 (1)	0 (0)	1 (1)	0 (0)	0 (0)	0 (0)
Low albuminemia	1 (1)	0 (0)	1 (1)	0 (0)	0 (0)	0 (0)	0 (0)	0 (0)	0 (0)
Nausea/anorexia/pain/ascites	4 (2)	2 (2)	6 (2)	0 (0)	0 (0)	0 (0)	0 (0)	0 (0)	0 (0)

therapy would be the best therapeutic option for patients who have tumors that preclude currently available local therapies because of tumor size, macroscopic vascular invasion, or deep tumor location.

According to the BCLC classification, the 5-year overall survival rate of patients in the operable group was 67.6%. This survival rate is comparable to reported data associated with hepatic resection.[21] It is noteworthy that the overall survival rate of patients classified with stage C disease at 5 years was 30.6% in the current study; this is far superior to other reported data.[21] Patients in this stage have macroscopic vascular invasion and/or extrahepatic metastasis. According to the BCLC classification, these patients usually are excluded from curative treatments and receive either TACE or sorafenib. In the current study, most of patients with stage C disease had macroscopic vascular invasion without extrahepatic metastasis. They were received proton and carbon ion therapies with curative intent, and the local control rates for these patients exceeded 80% (Table 4). These results suggest that some of patients with BCLC stage C disease may benefit from more aggressive local therapies, such as particle therapy.

Most of the treatment-related toxicities in the current study were transient, easily managed, and acceptable. Rib fracture and dermatitis were observed frequently in patients who were treated during the early period at our center. Most of these patients, including 1 patient with grade 4 dermatitis, were treated with only 1 portal to obtain an adequate spread-out Bragg peak. Thereafter, we used 2 or more portals and rarely observed such complications. Regarding intrahepatic structure-related complications, no studies, including

ours, have reported blood vessel-related complications. This is a distinct advantage of particle therapy over other local therapies and supports our proposal that tumors in perivascular locations are appropriate candidates for particle therapy. In contrast, although less common, bile duct complications, including biloma and stenosis, have been reported in several studies.[16] In the current study, biloma formation was observed in 1 patient whose tumor was adjacent to the porta hepatis. The bile duct may stand as the single greatest obstacle of intrahepatic structures after particle therapy. It is almost impossible to predict bile duct complications before treatment; thus, tumors adjacent to the porta hepatis should be treated with caution.

Grade 2 or greater gastrointestinal ulceration was observed in 5 patients whose tumors were adjacent to the gut. To minimize toxicity in these patients, we reduced the fraction size and initiated proton pump inhibitors immediately after treatment; and, ultimately, we were able to prevent the development of severity. The proximity of the gut is an important consideration in selecting particle therapy for patients with HCC. We introduced operative placement of a spacer between the tumor and the gut before particle therapy as a countermeasure for this limitation to ensure safe irradiation.[37,38]

To our knowledge, this is the first study to assess the clinical treatment results from both proton therapy and carbon ion therapy. However, our study has some important limitations: 1) the results of this study were achieved retrospectively and not through randomized or controlled trials; 2) during the study period, we used different treatment protocols for proton therapy and carbon ion therapy; and 3) the RBE of carbon ion beams for HCC